Production and Precipitation Hardening of Mg-Ca-Zn-Co Alloy for Tissue Engineering

Ilven Mutlu

Istanbul University, Metallurgical and Materials Engineering Department, Istanbul, Turkey

Correspondence: Ilven Mutlu. Istanbul University, Metallurgical and Materials Engineering Department, Istanbul, Turkey

<imutlu@istanbul.edu.tr>

Abstract. In this study, Mg-Ca-Zn-Co alloy specimens for biomedical applications were produced by the powder metallurgy method. The Mg-Ca-Zn-Co alloy could be used as a scaffold material in tissue engineering applications. Electrochemical corrosion behavior of the specimens was investigated in simulated body fluid environment. Electrochemical corrosion resistance of the specimens was increased with increasing Zn and Ca contents of the alloy up to an optimum composition and then decreased. Optimum values for Ca and Zn additions were about 0.7 wt.% and 3.0 wt.% respectively. Young's modulus values of the specimens were determined by nondestructive ultrasonic measurement. Alloying element addition increased the Young's modulus of the specimens. Precipitation hardening of the Mg-Ca-Zn-Co alloy increased the Young's modulus and the corrosion rate of the specimens.

Key words: Mg-Ca-Zn-Co, Young's modulus, Corrosion, Scaffold, Precipitation hardening

Scaffold provides support for cells, and its architecture defines the shape of the new tissue. Scaffold material should be osteoconductive, biodegradable, and strong enough. Several scaffold materials, including hydroxyapatite and polymers, have been investigated. Brittle nature of ceramics and low strength of polymers have limited applicability of these materials. Stainless steels, Co alloys, and Ti alloys have been studied in hard tissue implants. However, they cannot degrade [1, 2].

Mg has been recognized as a material for bone implants because it is biodegradable. Mg has potential as a scaffold material for bone substitute applications. Toughness of the Mg is greater than ceramics, whereas Young's modulus is close to bone that avoids stress shielding. Mg is essential to metabolism and found in the bone tissue. Mg shows poorer corrosion resistance in Cl^- containing environments. As a result, Mg alloys could be developed as a biodegradable metal, with their fast corrosion rate in physiologic environment [1-7].

It is essential to control corrosion rate and to improve strength of the Mg. Oxides or hydroxides that formed during degradation enhance activity of osteoblast during bone regeneration [1-3]. Mg alloys indicate close elastic modulus to bone compared with Ti alloys, better ductility than hydroxyapatite, and higher strength than polymers. Another important performance is the degradation rate. It not only matters to tissue healing period but also influences the loss of the mechanical properties during degradation [2].

Studies on biomedical Mg alloys focused on two aspects. First is corrosion and biocompatibility evaluation. Most Mg alloys contain neurotoxicant Al and hepatotoxic rare earth elements. Another highlight is exploration of new Mg alloy system containing nontoxic element. The main issue of the Mg is related to its low strength and poor corrosion resistance. Mechanical integrity is destroyed

doi:10.1684/mrh.2017.0417

Pour citer cet article : Mutlu I. Production and Precipitation Hardening of Mg-Ca-Zn-Co Alloy for Tissue Engineering. *Magnes Res* 2017 ; 30(1) : 16-27 doi:10.1684/mrh.2017.0417

before tissue has healed. Some Mg alloys, such as AZ31, and WE43 have been attempted as biomaterials. For these alloys, Al, Mn, Zr elements are employed to improve mechanical and corrosion properties. However, these products result in negative effects on humans [2-6].

There are some drawbacks of Mg. First, yield strength of Mg is low. The second drawback is anisotropy. Third, Mg alloys must be formed above 300 °C as they lack formability. High temperatures result in grain growth. Precipitation during hot forming can make the grain size finer. Microstructure can be refined by pinning of the grain boundaries by particles. Due to biocompatible element Zn, Mg-Zn alloys are of high interest as implant materials. Zn is a grain refiner and enhances strength of the Mg alloys. Mg-Zn alloys revealed improved corrosion properties, which was attributed to the ability of Zn to form precipitates. Low volume fractions of MgZn decrease the corrosion rate, whereas larger volume fractions promote microgalvanic corrosion. Zn contents up to 5.6 wt. % improved the corrosion properties. Also, since maximum solubility of Zn in Mg is 8.4 wt. %, a considerable amount of Zn can be retained in a solid solution in Mg [3-5]. Mg-Zn alloys offer constant degradation rate owing to homogeneous microstructure. Zn improves corrosion resistance but also enhances mechanical properties. Mg-Zn alloys possess the highest capacity for aging due to the segregation of an intermediate phase [1-6].

Ca is an element in refining the microstructure and precipitates in Mg alloys, and in improving strength and corrosion resistance. Formation of a calcium-phosphate layer was observed during immersion in simulated body fluid beneficial on cell adhesion and corrosion protection [3-5]. Mg-Zn is a precipitation hardenable alloy, in which solubility of Zn in the Mg decreases with increasing temperature. The radius of the Zn atom is smaller than that of Mg, while the radius of Ca is larger than that of Mg. Another feature is that mixing enthalpy between solute elements is negatively large. During aging, decomposition of super-saturated solid solution results in the formation of second-phase precipitates. Difference in atomic size and negative heat of mixing favors the formation of GP zones [7-10]. Additions of Co to the Mg-Zn alloy raised the eutectic temperature and induced a response to aging. Microstructure of Mg-Zn-Co is finer than that of Mg-Zn. Intermetallic particles are refined by Co. Addition of Co permits use of higher temperature for solution treatment, which leads to larger supersaturation of Zn atoms and higher concentration of vacancies in Mg grains after solution and quenching, which enhance nucleation and increase density of precipitates. Increase in eutectic temperature permits use of higher solution temperature, ensuring greater supersaturation of Zn [9-11]. Kinetics of the aging is accelerated in Co-containing alloy. Co segregates into eutectic intermetallic particles or reacts with Mg to form $MgCo_2$. Co has partitioned into Mg-Zn phases rather than forming $MgCo_2$ phase. As a result of increased Zn in the Mg solid solution, a larger volume fraction of precipitates could be formed during aging, which leads to larger driving force for precipitation. Increased driving force and enhanced diffusion rate of solutes leads to higher nucleation rates of precipitates [9-11].

Bobe *et al.* [12] fabricated a biocompatible, biodegradable, open-porous, mechanically adaptable scaffold from Mg alloy by liquid phase sintering. Specimens of short fibers were evaluated under in vitro and in vivo conditions. The in vitro environment influenced the corrosion rates compared with in vivo. The culture media composition influences the ionic composition of the extract by selectively dissolving ions from specimens. Aghion *et al.* [13] produced Mg foams by powder metallurgy as a scaffold for drug delivery applications. The amount and delivery time of the released drug was controlled by a space holder. Microtomography was used to evaluate the structure. Corrosion behavior was characterized by the immersion test. Absorption of gentamicin was obtained by immersing foams in gentamicin solutions. Results show that the release profile of gentamicin was in accord with common dissolution kinetics of an active ingredient from polymeric drug delivery systems. Wen *et al.* [14] produced Ti and Mg foams by powder metallurgy route for scaffold applications. Starting materials were Mg and Ti powders. Ammonium hydrogen carbonate and carbamide particles were used as a space holder. Pore size was in the range of 200-500 μm. Porosity contents were 78 % and 50 % for Ti and Mg foams, respectively. Yusop *et al.* [15] used the computation-aided solid free-form method as a method for scaffold production. With further optimization in topologically ordered porosity design exploiting material property and fabrication technique, porous biodegradable metals could be the potential materials for scaffolds. Aghion *et al.* [16] characterized the effect of porosity on the corrosion resistance of

Mg foams in NaCl and in the phosphate buffer saline solution. Foams were produced by the powder metallurgy method by using a space holder. Machined chips were used as raw material. Results demonstrate that the porosity has a significant effect on the corrosion behavior. Wen *et al.* [17] investigated the mechanical properties of porous Mg with the porosity of 35-55 % and the pore size of 70-400 μm. Results indicated that the Young's modulus increases with decreasing porosity and pore size. Mechanical properties of the specimens were in a range of those of human bone. It is suggested that the porous Mg is one of the promising scaffold materials for hard tissue regeneration.

Until now, there has been limited study on the production of Mg-Ca-Zn-Co alloy for biomedical applications produced by powder metallurgy. In this study, the Mg-Ca-Zn-Co alloy was produced for biomedical applications by the powder metallurgy method. Although cast Mg-Ca-Zn/Mg-Ca-Zn-Co alloys were studied [3-5], studies on powder metallurgy Mg-Ca-Zn-Co alloy are limited. Corrosion behavior of the specimens was examined in a simulated body fluid. In addition, Young's modulus of the specimens was determined. Since the corrosion rates found in the literature are not as low as required for the application within the body, further investigations regarding an improved alloy composition design are required. In the range of the low alloyed Mg-based alloy, the effect of alloying elements on the degradation has not been fully investigated. In this study, both alloying elements Co and Zn were varied.

Experimental

Specimen production

Specimens were produced by the powder metallurgy method using Mg, Ca, Zn, and Co powders (Alfa Aesar, USA). Purity of the powders was >99.5 wt. %. Mean particles size of the powders was -325 mesh (about 34 μm). In the alloy preparation stage, 0.3, 0.7, and 1.0 wt. % Ca, 1.0, 3.0, 5.0, and 8.0 wt. % Zn, and 0.3, 0.6 wt. % Co powder were added to the Mg powder. The powder mixtures were ball-milled, to prepare the alloys, using a ball-milling machine. The mixture was loaded in a hardened steel vial with ZrO_2 balls (3 mm of diameter) to give a ball-to-powder weight ratio of 10:1. The powders were mechanically alloyed for 4 hours with a rotational speed of 400 rpm without addition of any process control agent to avoid contamination of the powder. Binder for green strength was polyvinylalcohol (PVA). Metal powders were mixed with 1.5 wt. % PVA. Mixtures were compacted at 250 MPa into cylindrical specimens with a diameter of 12 mm and heights of 15-17 mm. The sintering cycle was consisted of heating at a rate of 5 °C/minutes to 400 °C (debinding) with a dwell time of 40 minutes, followed by heating at a rate of 11 °C/minutes to sintering temperatures. Specimens were sintered at 580 °C for 60 minutes in argon atmosphere. The precipitation hardening heat treatment was consisted of two steps. Specimens were heated to 400 °C for 1 hour duration followed by quenching. Quenched specimens were precipitation hardened at 200 °C for 1 hour.

Microstructure characterization and ultrasonic testing

Microstructure of the specimens was examined by field emission gun-scanning electron microscopy (FEG-SEM), FEI Quanta FEG 450. X-ray diffraction (XRD) analysis (Rigaku D/Max-2200/PC) was used to characterize the alloys. Among nondestructive techniques, ultrasonic testing is the most used. Ultrasonic velocity is related to Young's modulus and density of material. Ultrasonic wave is influenced by microstructure, which determines mechanical properties. Hence, a possibility exists for the characterization of microstructure and mechanical properties. Ultrasonic wave velocities were measured by using the pulse-echo method. A pulse-receiver-type ultrasonic instrument (General Electric, USMGo), with 4 MHz normal beam wave transducer, was used for the ultrasonic velocity measurements. Young's modulus of the specimens was determined by ultrasonic velocity measurements and the density of the materials. Young's modulus (E) was calculated by using the following equation [18] by the material density (ρ), ultrasonic longitudinal velocity (V_L), and ultrasonic transverse velocity (V_T). Densities of the specimens were determined by the mass over volume method.

$$E = \rho V_T{}^2 \frac{3V^2{}_L - 4V_T{}^2}{V_L{}^2 - V_T{}^2}$$

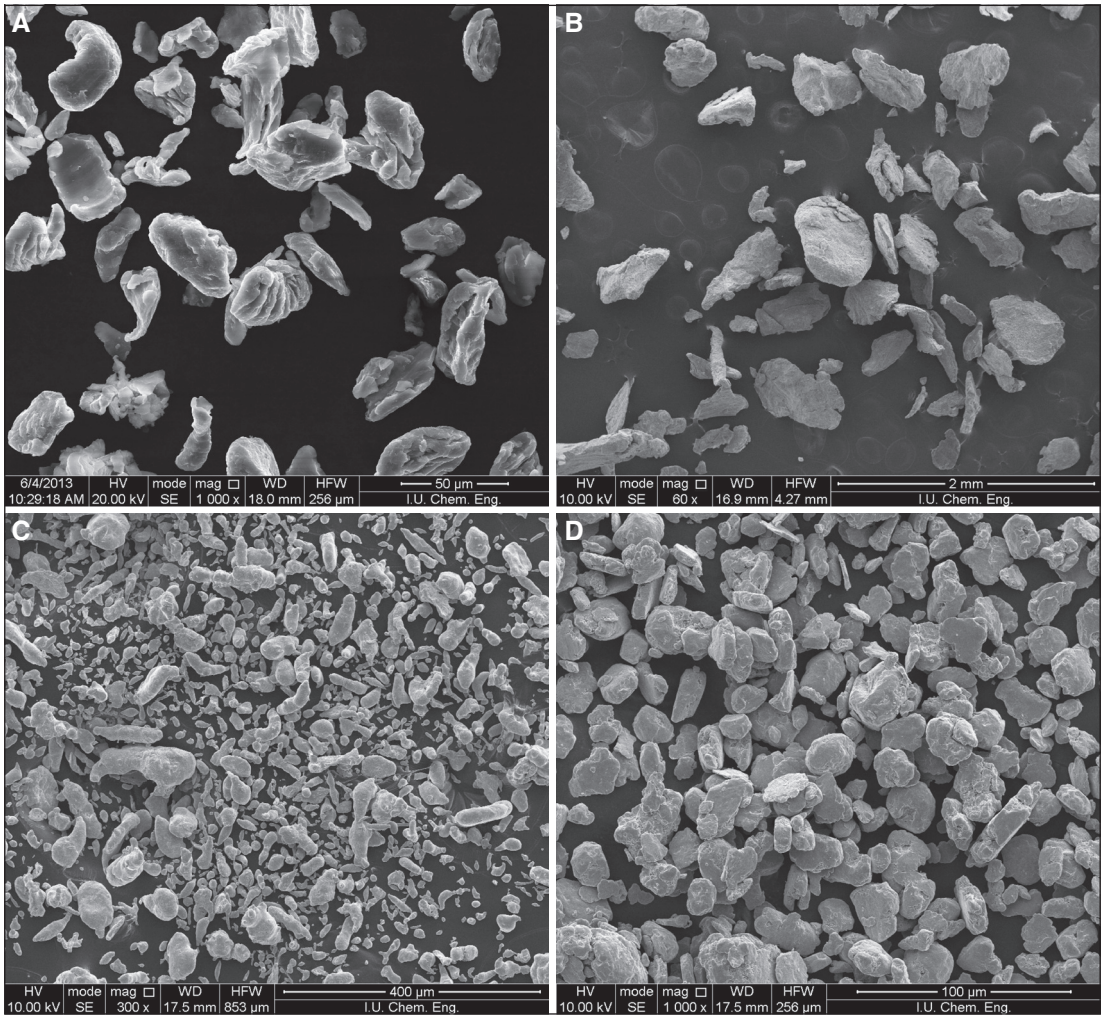

Figure 1. SEM images of the **(A)** Mg, **(B)** Ca, **(C)** Zn, and **(D)** Co powders.

Simulated body fluid preparation

A simulated body fluid (SBF) solution was prepared from chemicals (Merck, Germany) according to the literature [19-25]. Amounts of the chemical reagents were 8.03 g/L NaCl, 0.29 g/L $CaCl_2$, 0.22 g/L KCl, 0.31 g/L $MgCl_2$ 6 H_20, 0.23 g/L K_2HPO_4 3 H_20, 0.35 g/L $NaHCO_3$, 0.07 g/L Na_2SO_4, 39 mL 1.0 M HCl, 6.11 g/L tris, and appropriate amount 1.0 M HCl. The pH of the simulated body fluid (SBF) was adjusted to 7.40.

Electrochemical corrosion study

Electrochemical corrosion studies were carried out using a potentiostat (Interface 1000 Potentiostat/Galvanostat/ZRA, Gamry Instruments Inc., USA) controlled by a personal computer. The volume of the glass corrosion test cell was 1000 mL. A conventional three-electrode system with a high-density graphite rod as a counter electrode, a saturated calomel electrode (SCE) as a reference electrode, and a specimen as a working electrode was used. Data acquisition was carried

out through a computer software (Framework, Version 6.04, Gamry Instruments, USA), whereas data analysis was carried out by Echem Analyst Software, Version 6.04, Gamry Instruments, USA. Specimens were prepared by being cut and then mounted into epoxy resin. So, only circular cross section with a diameter of about 10 mm of the specimens was exposed to the solution. The specimens were connected to a copper wire. All the corrosion experiments were carried out at room temperature. Open circuit potential (OCP) of the specimens was measured before carrying out the electrochemical corrosion experiments. The open circuit potential (OCP) level was measured for durations of 2 to 3 hours, until the OCP was stabilized. Tafel curves were obtained by polarizing the specimens from -250 mV to +250 mV (vs. SCE), with respect to the OCP, at a scan rate of 1.0 mV/s. The corrosion rate was calculated by the software (DC105, Gamry). Calculations were based on the numerical curve fit to the Butler-Volmer equation. Corrosion rate (mm year^{-1}), corrosion potential (E_{corr}), corrosion current density (I_{corr}), the anodic beta Tafel constant (β_{anode}), the cathodic beta Tafel constant ($\beta_{cathode}$) values were calculated. Beta (β) coefficients give kinetic information about anodic and cathodic reactions. In the linear polarization resistance (LPR) test, the specimens were polarized from -20 mV to +20 mV (vs. SCE), at a scanning rate of 0.125 mV/s, to measure polarization resistance and corrosion rate of the specimens.

Cyclic polarization tests were carried out from -500 mV (vs. SCE) to apex potential and to final potential, which was 0 mV (vs. SCE). The forward and reverse polarization scan rates were 5 and 2.5 mV/s, respectively. The cyclic (forward and reverse) polarization technique was used to evaluate tendency to localized corrosion (pitting) in corrosive environment. Considerable hysteresis between the forward and reverse polarization sweeps is an indication of the pit formation.

Static immersion test

Specimens were exposed to simulated body fluid (SBF) solution at room temperature for times up to 120 hours. Samples were immersed in a 500 mL solution. Surface area of each specimen was equal in immersion tests. The solution volume-to-surface area ratio was constant in all the tests. Inductively coupled plasma-mass spectrometer, ICP-MS (Thermo Scientific Elemental X Series 2), was employed to measure the Mg ions. Weight loss/gain values of the specimens were determined by the gravimetric method. After different soaking periods, the specimens were removed from the SBF solutions. Then the specimens were rinsed with distilled water and then dried. The dried specimens were weighed and weight gain was determined. The immersed samples were cleaned using a solution of 180 g/L chromic acid to remove the surface corrosion product, and then rinsed with ethanol, dried in air, and finally weighed to calculate the weight loss value [26-28].

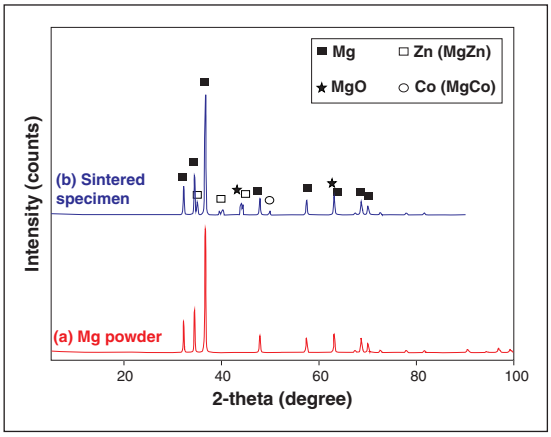

Figure 2. XRD patterns of the **(A)** Mg powder and **(B)** sintered Mg alloy specimen.

Results and discussion

Microstructure

In the present study, the Mg-Ca-Zn-Co alloy specimens were produced by the powder metallurgy method for biomedical implant (scaffold) applications. *Figure 1* shows the SEM images of the (*figure 1A*) Mg, (*figure 1B*) Ca, (*figure 1C*) Zn, and (*figure 1D*) Co powders.

Figure 2 shows the x-ray diffraction (XRD) patterns of the (*figure 2A*) Mg powder and (*figure 2B*) sintered Mg alloy specimen. As-received Mg powder consists of Mg phase. Sintered Mg-Ca-Zn-Co alloy specimen was mainly consisted of Mg phase. Some Ca phase, Co phase (MgCo), Zn phase

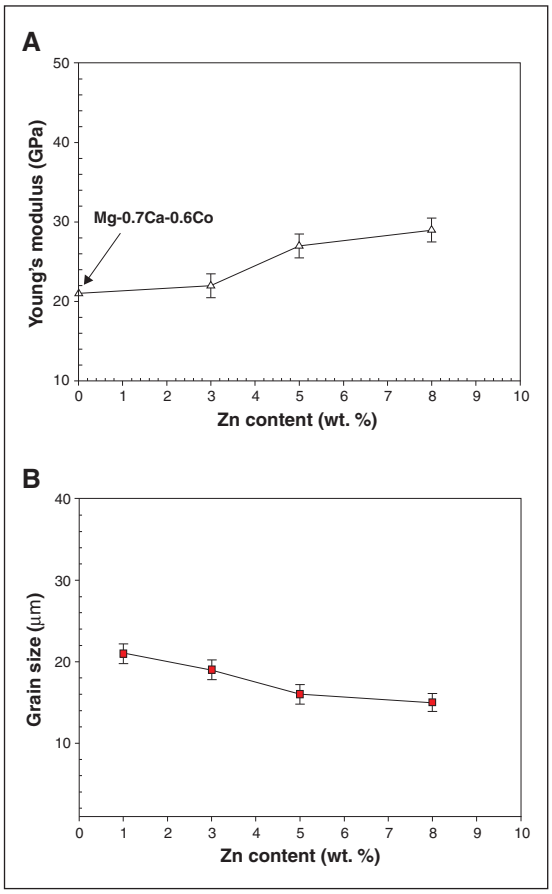

Figure 3. Effect of Zn content of the alloy on the **(A)** Young's modulus and **(B)** grain size.

(MgZn), and oxide (MgO) were also formed on the surfaces of the sintered Mg-Ca-Zn-Co alloy specimens.

Mechanical properties

Addition of Co to the alloy can increase the Young's modulus of the specimens. Precipitation hardening involves dislocation particle interaction, load transfer from matrix to the particles, generation of dislocation due to the difference between thermal expansions of matrix and the particles, generation of dislocation due to geometric requirements in deformation. These phases become sites to pin movement of dislocations. Strength is improved due to the fine precipitates. Addition of Zn could refine the grain size and improve mechanical properties. Addition of Co to the Mg alloy allows use of higher solution treatment temperatures that can lead to higher concentrations of Zn atoms and vacancies, which can increase precipitate number and precipitation hardening response [1-3, 9, 10].

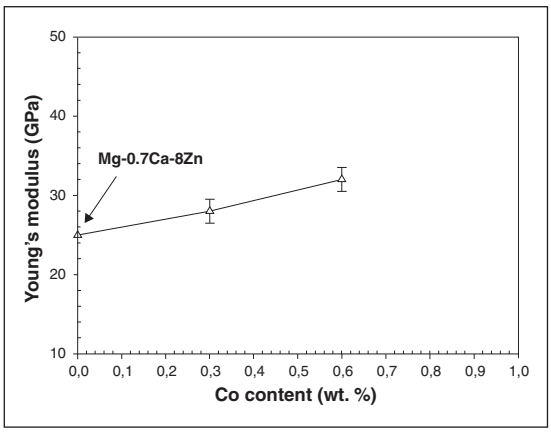

Figure 4. Effect of Co content of the alloy on the Young's modulus.

Improved strength was attributed to the fine grain size and homogeneous second precipitates. Zn can be added to the Mg alloy as a grain refiner. Increasing the Zn content of the alloys can produce a decrease in the grain size and improve mechanical properties. *Figure 3* shows the effect of Zn content of the alloy on the (*figure 3A*) Young's modulus of the sintered specimens and (*figure 3B*) grain size of the sintered specimen. As seen from *figure 3A*, Zn addition to the alloy increased the Young's modulus of the sintered specimens. *Figure 3B* shows the effect of Zn content of the alloy on the grain size, which is determined by ultrasonic velocity measurements, of the sintered specimen. As seen from *figure 3B*, Zn addition to the alloy decreased the grain size of the sintered specimens. Grain size decreases with increasing Zn content. Zn resolves in the Mg when Zn content is 1-2 wt. %, which can improve strength by solid-solution strengthening. When Zn is 4 or 6 wt. %, Mg-Zn phases precipitated from matrix. Such an effect enhances the strength by dispersion strengthening. Zn can act as a constituent to refine microstructure of the matrix and to improve the strength [1-3, 9, 10].

Figure 4 shows the effect of Co content of the Mg-Ca-Zn-Co alloy on the Young's modulus of the specimens. As seen from *figure 4*, Co addition increased the Young's modulus of the specimens.

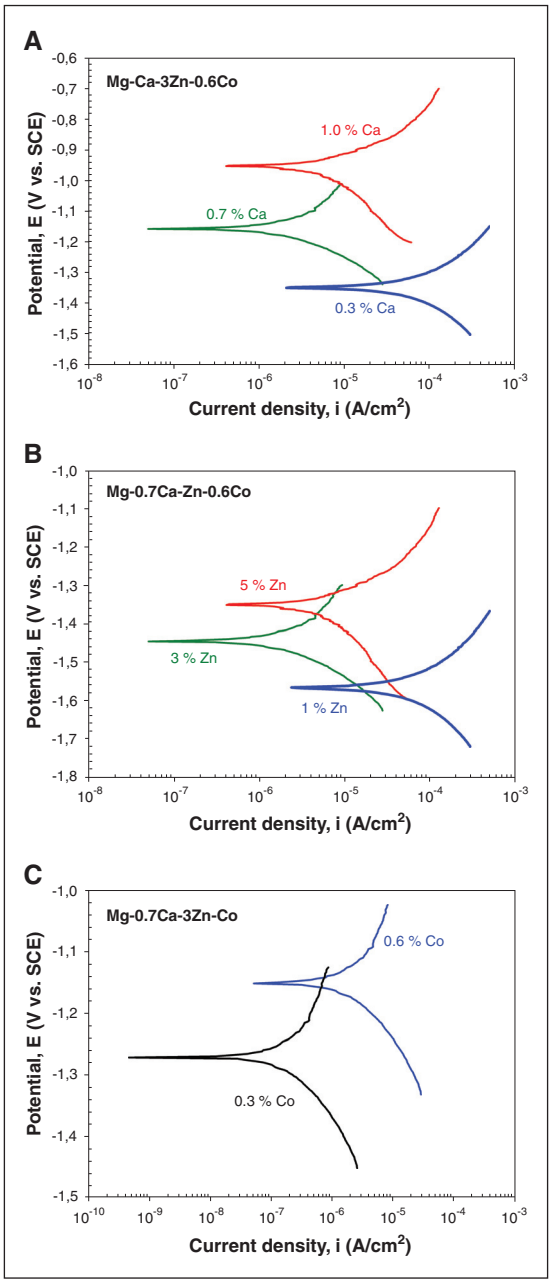

Figure 5. Effect of **(A)** Ca, **(B)** Zn, **(C)** Co contents, and **(D)** heat treatment of the alloy on the Tafel curves.

Increasing Co content of alloy from 0.3 wt. % to 0.6 wt. % increased the Young's modulus of the Mg alloy specimens from about 28 GPa to 32 GPa.

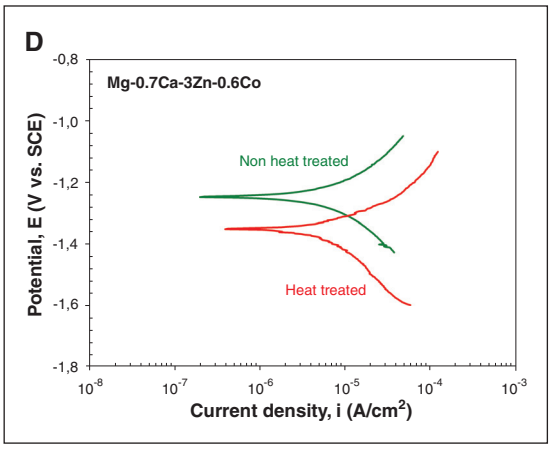

Figure 5. *(Continued).*

High strength and low Young's modulus that are compatible with the bone are essential for the selection of biomedical implant (hard tissue) materials. If the Young's modulus of an implant material is compatible with cancellous bone, bone growth may be stimulated and a healthy bone structure maintained to avoid bone resorption.

Electrochemical corrosion tests

Tafel tests

Tafel curves were used to examine the electrochemical corrosion behavior of the specimens. *Figure 5* shows the effect of Ca content, Zn content, Co content of the Mg-Ca-Zn-Co alloy, and heat treatment (precipitation hardening) on the Tafel curves. As shown in *figure 5*, increasing Ca, Zn, and Co contents of the alloy increased the electrochemical corrosion potential and increased the corrosion current density of the specimens. As shown in *figure 5D*, heat treatment (precipitation hardening) decreased the electrochemical corrosion potential and increased the corrosion current density of the specimens.

Ca addition to the Mg-Zn-Co alloy reduced the electrochemical corrosion rates of the alloy. However, larger amounts of the Ca above about 0.7 wt. % increased the electrochemical corrosion rate (current density) of the alloy. Addition of Zn to the Mg-Ca-Co alloy decreased the electrochemical corrosion rates of the alloy. However, larger amounts of the Zn above 3 wt. % increased the electrochemical corrosion rates (current density).

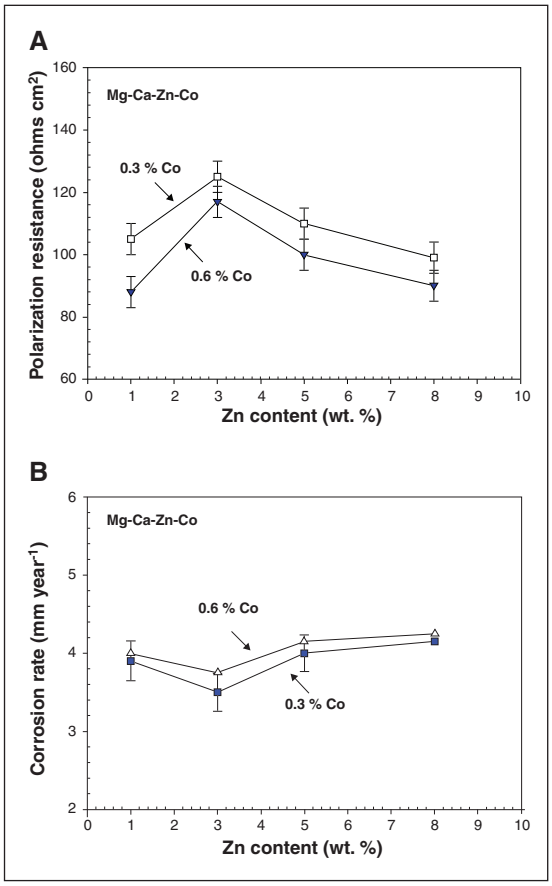

Figure 6. Effect of Zn and Co contents of the alloy on the **(A)** polarization resistance and **(B)** corrosion rate.

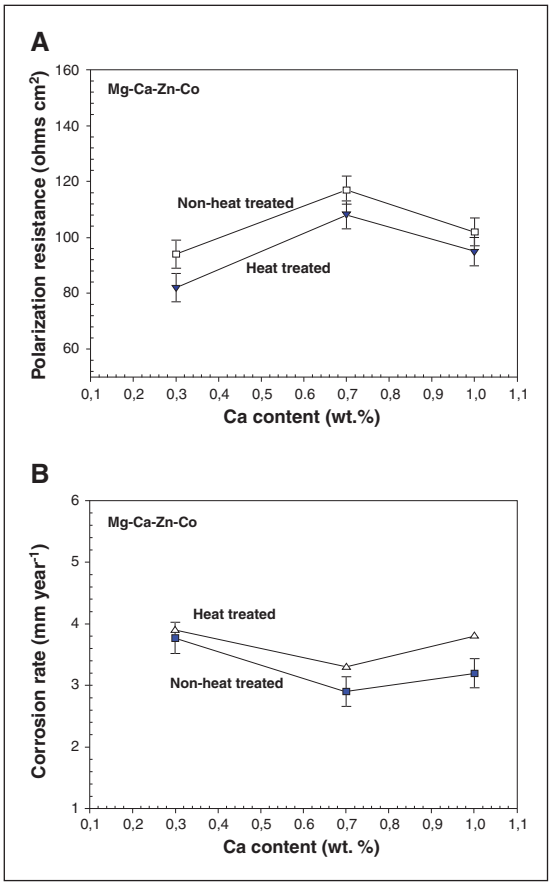

Figure 7. Effect of Ca contents and heat treatment of the alloy on the **(A)** polarization resistance and **(B)** corrosion rate.

These results were in agreement with the literature [1-3, 9, 10].

Table 1 shows the corrosion parameters obtained from the Tafel curves. Corrosion rate (mm year^{-1}), corrosion potential (E_{corr}), corrosion current density (I_{corr}), the anodic beta Tafel constant (β_{anode}), and the cathodic beta Tafel constant ($\beta_{cathode}$) values are given.

Linear polarization tests

Figure 6 shows the effect of Zn and Co contents of the Mg-Ca-Zn-Co alloy on the polarization resistance and corrosion rate, whereas *figure 7* shows the effect of Ca contents of the Mg-Ca-Zn-Co alloy and heat treatment (precipitation hardening) on the polarization resistance and corrosion rate. In general, polarization resistance is connected with kinetic phenomena at the metal-solution interface. In general, polarization resistance and corrosion rate values characterize the protection degree of the passive surface oxide layer.

As seen from *figure 6*, addition of Zn to the Mg-Ca-Co alloy decreased the electrochemical corrosion rates of the alloy. However, larger amount of the Zn above 3 wt. % increased the electrochemical corrosion rates. Addition of Zn increased the polarization resistance. Larger amount of the Zn above 3 wt. % decreased the polarization resistance of the specimens. Meanwhile, increasing the Co content of the Mg-Ca-Zn-Co alloy from 0.3 wt.% to 0.6 wt.% decreased the polarization resistance and increased the corrosion rate of the specimens.

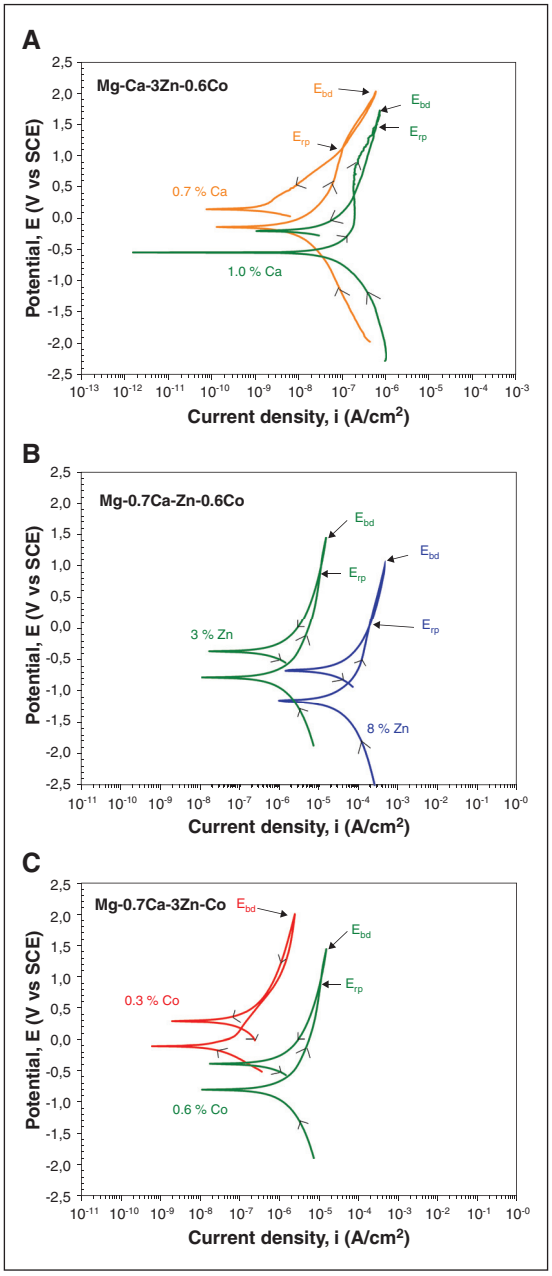

Figure 8. Effect of **(A)** Ca, **(B)** Zn, **(C)** Co contents, and **(D)** heat treatment of the alloy on the cyclic polarization curves.

As seen from *figure 7*, addition of Ca to the Mg-Zn-Co alloy decreased the electrochemical corrosion rates of the alloy. However, larger amount

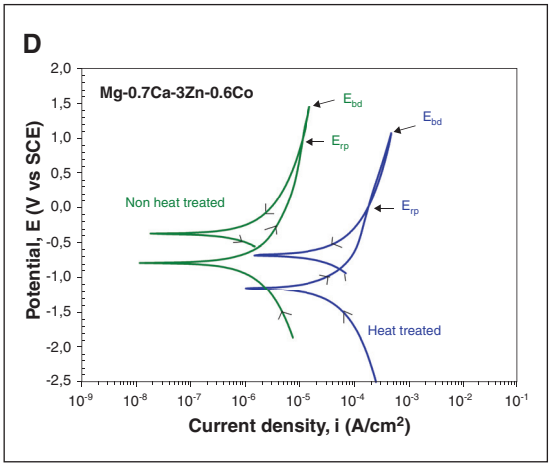

Figure 8. *(Continued).*

of the Ca above 0.7 wt. % increased the electrochemical corrosion rates. Addition of Ca increased the polarization resistance. Larger amount of the Ca above 0.7 wt. % decreased the polarization resistance of the specimens. Meanwhile, heat treatment (precipitation hardening) slightly increased the corrosion rate and decreased the polarization resistance of the specimens.

Cyclic polarization test

Cyclic polarization is used to qualitatively evaluate tendency to localized corrosion (pitting or crevice). In general, hysteresis between forward and reverse sweeps during cyclic polarization is an indication of localized corrosion (pitting). *Figure 8* shows the effect of Ca, Zn, and Co contents of alloy and heat treatment (precipitation hardening) on the cyclic polarization curves. As seen from *figure 8*, increasing Ca, Zn, and Co contents of the alloy decreased the localized corrosion resistance of the specimens. As seen from *figure 8*, there was not a considerable hysteresis (loop) in the cyclic polarization curves, with increasing Ca, Zn, and Co contents of the alloy. Precipitation hardening slightly decreased the localized corrosion resistance of the alloy.

Cyclic polarization curves were also analyzed in terms of breakdown potential (E_{bd}), which is top of the loop in the forward polarization region, and repassivation potential (E_{rp}), which is the intersection point of the forward and reverse polarization curves. Breakdown potential corresponds to potential for new pit formation

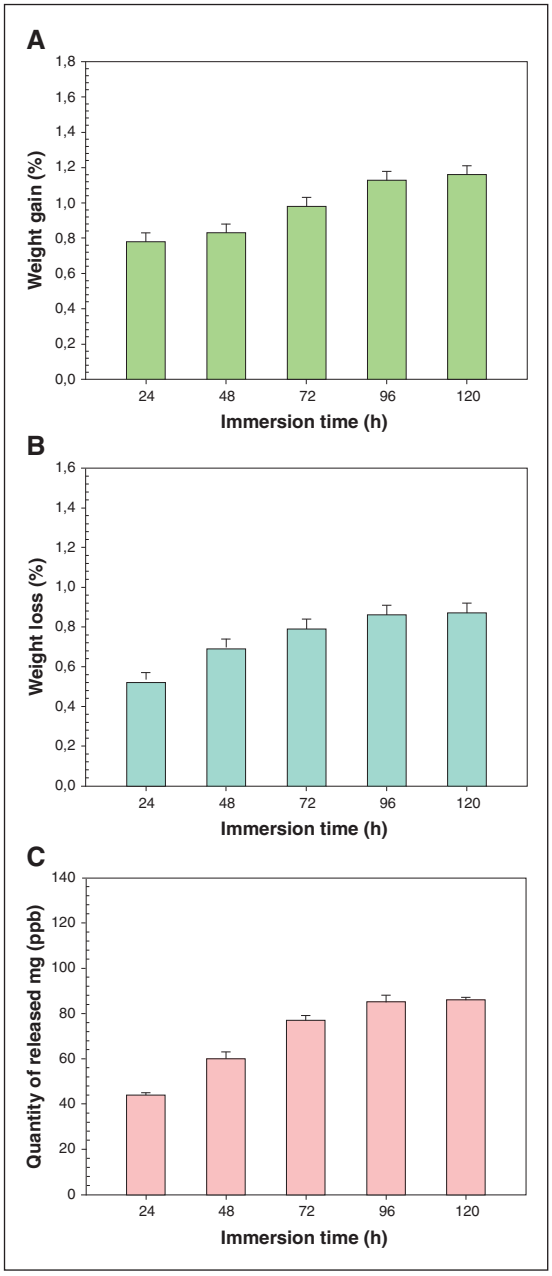

Figure 9. Effect of immersion time on the **(A)** weight gain, **(B)** weight loss, and **(C)** Mg ion release of the alloy in SBF.

and stable pit growth. In general, increase in the resistance to pitting is associated with increase in the E_{bd}. Pits are initiated above E_{bd}, but if pits were once initiated they propagate at all potentials above E_{rp}. Thus, E_{rp} is used in the design as protection potential. A metal will resist to pitting if its potential is kept below E_{rp}. Below E_{rp} all the pits repassivate. Increasing Zn and Co contents decreased the E_{bd} and E_{rp}.

Static immersion test

Determination of the interaction of biomaterials with human body fluids is important. *Figure 9* shows the effect of immersion time on the (*figure 9A*) weight gain, (*figure 9B*) weight loss, and (*figure 9C*) Mg ion release of the alloy in simulated body fluid (SBF) environment. As seen from *figure 9A*, weight gain was increased with increasing immersion time in SBF. As seen from *figure 9B* weight loss was also increased with increasing immersion time.

Weight loss was observed in the specimens, which cleaned using chromic acid. Weight loss of the Mg alloys in the SBF environments happens as a result of dissolving of Mg by the reaction between Mg and SBF solutions. Weight gain was observed in the specimens, which did not clean using chromic acid. Weight gain of the Mg alloys in SBF happens as a result of formation of insoluble corrosion (precipitation) products on the specimen surface [26-28].

Figure 9C shows the effect of immersion time on the Mg ion release in the simulated body fluid (SBF) solution. It can be seen from the *figure 9C* that increasing immersion time increased the quantities of released metal (Mg) ions.

Conclusions

In this study, Mg-Ca-Zn-Co alloy specimens for biomedical applications were produced by the powder metallurgy method. The Mg-Ca-Zn-Co alloy could be a scaffold material for hard tissue generation in tissue engineering applications. Electrochemical corrosion behavior of the specimens was examined in the simulated body fluid. Corrosion behavior of the specimens was slightly increased with increasing Zn and Ca contents of the Mg-Ca-Zn-Co alloy up to an optimum composition and then decreased. Addition of Zn to the Mg-Ca-Co alloy decreased the corrosion rates of the alloy. However, larger amount of the Zn above 3.0 wt. % increased the corrosion rates. Addition of Ca to the Mg-Zn-Co alloy decreased

Table 1. The corrosion parameters obtained from the Tafel curves

Parameter		β_{anode} (V/decade)	$\beta_{cathode}$ (V/decade)	E_{corr} (V vs SCE)	I_{corr} (A/cm^2)	Corrosion Rate (mm $year^{-1}$)
Ca	0.3 % Ca	0.15	0.12	-1.36	9.10^{-5}	5.85
	0.7 % Ca	0.14	0.07	-1.14	3.10^{-6}	1.11
	1.0 % Ca	0.65	0.47	-0.94	10.10^{-6}	1.55
Zn	1.0 % Zn	0.43	0.19	-1.57	8.10^{-5}	4.25
	3.0 % Zn	0.68	0.38	-1.45	3.10^{-6}	1.34
	5.0 % Zn	0.03	0.11	-1.35	2.10^{-5}	5.93
Co	0.3 % Co	0.24	0.20	-1.27	3.10^{-7}	2.01
	0.6 % Co	0.11	0.54	-1.15	3.10^{-6}	2.13
Aging	Heat trated	0.21	0.55	-1.36	9.10^{-6}	2.18
	Non-heat treated	0.44	0.59	-1.24	10.10^{-6}	2.09

the corrosion rates. However, larger amount of the Ca above 0.7 wt. % increased the corrosion rates. Increasing the Co content of the Mg-Ca-Zn-Co alloy from 0.3 to 0.6 wt.% increased the corrosion rate of the specimens. Precipitation hardening of the Mg-Ca-Zn-Co alloy increased the corrosion rate. Mechanical properties (Young's modulus) of the specimens were determined. Zn and Co additions to the alloy increased the Young's modulus of the specimens. As Mg is a highly active metal, Ca addition to the Mg prevented the oxidation of the specimens during sintering. Electrochemical corrosion behavior of the Mg alloy can be optimized with alloying. Young's modulus of the alloys can also be improved to the desired levels for biomedical implant applications. As a result, the Mg-Ca-Zn-Co alloy can be used as a scaffold material in tissue engineering applications.

Disclosure

Financial support: This research work was supported by the Scientific and Technological Research Council of Turkey (TÜBİTAK), Grant No: 214M438. This work was also supported partially by Scientific Research Projects Coordination Unit of Istanbul University, Project numbers of 42922 and 42796. Conflict of interest: none.

References

1. Seyedraoufin ZS, Mirdamadi S. Synthesis, microstructure and mechanical properties of porous Mg-Zn scaffolds. *J Mech Behav Biomed Mater* 2013; 21: 1-8.
2. Gu XN, Zheng Y F. A review on magnesium alloys as biodegradable materials. *Front Mater Sci (China)* 2010; 4: 111-5.
3. Zander D, Zumdick NA. Influence of Ca and Zn on the microstructure and corrosion of biodegradable Mg-Ca-Zn alloys. *Corrosion Sci* 2015; 93: 222-33.
4. Park WW, You BS, Lee HR. Precipitation hardening and microstructures of rapidly solidified Mg-Zn-Ca-X alloys. *Met Mater Int* 2002; 8: 135-8.
5. Osorio-Hernandez JO, Suarez MA, Goodall R, Lara-Rodriguez GA, Alfonso I, Figueroa IA. Manufacturing of open-cell Mg foams by replication process and mechanical properties. *Mater Des* 2014; 64: 136-41.
6. Li H, Peng Q, Li X, Li K, Han Z, Fang D. Microstructures, mechanical and cytocompatibility of degradable Mg-Zn based orthopedic biomaterials. *Mater Des* 2014; 58: 43-51.
7. Friedrich HE, Mordike BL. *Magnesium Technology, Metallurgy, Design Data, Applications*. Germany: Springer-Verlag Berlin Heidelberg, 2006.
8. Iwaoka T, Nakamura M. Effect of compaction temperature on sinterability of magnesium and aluminum powder mixtures by warm compaction method. *Mater Trans* 2011; 52: 943-7.
9. Geng J, Gao X, Fang XY, Nie JF. Enhanced age-hardening response of Mg–Zn alloys via Co additions. *Scr Mater* 2011; 64: 506-9.
10. Jayaraj J, Mendis CL, Ohkubo T, Oh-ishi K, Hono K. Enhanced precipitation hardening of Mg-Ca alloy by Al addition. *Scr Mater* 2010; 63: 831-4.
11. Hono K, Mendis CL, Sasaki TT, Oh-ishi K. Towards the development of heat-treatable high-strength wrought Mg alloys. *Scr Mater* 2010; 63: 710-5.

12. Bobe K, Willbold E, Morgenthal I, *et al*. *In vitro* and *in vivo* evaluation of biodegradable, open-porous scaffolds made of sintered magnesium W4 short fibres. *Acta Biomater* 2013; 9: 8611-23.

13. Aghion E, Yered T, Perez Y, Gueta Y. The prospects of carrying and releasing drugs via biodegradable magnesium foam. *Adv Bio Mater* 2012; 12: B374-379.

14. Wen CE, Mabuchi M, Yamada Y, Shimojima K, Chino Y, Asahina T. Processing of biocompatible porous Ti and Mg. *Scr Mater* 2001; 45: 1147-53.

15. Yusop AH, Bakir AA, Shaharom NA, Abdul Kadir MR, Hermawan H. Porous biodegradable metals for hard tissue scaffolds: a review. *Inter J Biomater* 2012; 4: 641430.

16. Aghion E, Perez Y. Effects of porosity on corrosion resistance of Mg alloy foam produced by powder metallurgy technology. *Mater Charact* 2014; 96: 78-83.

17. Wen CE, Yamada Y, Shimojima K, Chino Y, Hosokawa H, Mabuchi M. Compressibility of porous magnesium foam: dependency on porosity and pore size. *Mater Lett* 2004; 58: 357-60.

18. Mutlu I, Ekinci S, Oktay E. Characterization of Heat Treated Titanium-Based Implants by Nondestructive Eddy Current and Ultrasonic Tests. *J Mater Eng Perform* 2014; 238: 2083-91.

19. Mutlu I. Electrochemical corrosion behavior of TiN-coated biomedical Ti-Cu Alloy foam in fluoride containing artificial saliva. *Metallurgical Mater Trans* 2014; 45A: 3640-9.

20. Kokubo T, Takadama H. How useful is SBF in predicting in vivo bone bioactivity? *Biomaterials* 2007; 27: 2907-15.

21. Zhecheva A, Sha W, Malinov S, Long A. Enhancing the microstructure and properties of titanium alloys through nitriding and other surface engineering methods. *Surf Coat Tech* 2005; 200: 2192-200.

22. Gurappa I. Characterization of different materials for corrosion resistance under simulated body fluid conditions. *Mater Charact* 2002; 49: 73-9.

23. Okazaki Y, Gotoh E. Comparison of metal release from various metallic biomaterials in vitro. *Biomaterials* 2005; 26: 11-21.

24. Lin FH, Hsu YS, Lin SH, Sun JS. The effect of Ca/P concentration and temperature of simulated body fluid on the growth of hydroxyapatite coating on Alkali-treated 316L stainless steel. *Biomaterials* 2002; 23: 4029-38.

25. Mutlu I. Sinter-coating method for the production of TiN-coated titanium foam for biomedical implant applications. *Surf Coat Tech* 2013; 232: 396-402.

26. Guo Y, Liu W, Ma S, *et al*. A preliminary study for novel use of two Mg alloys (WE43 and Mg3Gd). *J Mater Sci Mater Med* 2016; 27: 1-14.

27. Mousaa HM, Leea DH, Parka CH, Kima CS. A novel simple strategy for in situ deposition of apatite layer on AZ31B magnesium alloy for bone tissue regeneration. *Appl Surf Sci* 2015; 351: 55-65.

28. Xu L, Zhang E, Yin D, Zeng S, Yang K. *In vitro* corrosion behaviour of mg alloys in a phosphate buffered solution for bone implant applications. *J Mater Sci Mater Med* 2008; 19: 1017-25.